Materials Science-Poland, 32(4), 2014, pp. 555-564
http://www.materialsscience.pwr.wroc.pl/
DOI: 10.2478/s13536-014-0227-8

VERSITA

Chemical bath deposition synthesis and electrochemical properties of MnO_2 thin film: Effect of deposition time and bath temperature

A. A. AREF, Y.W. TANG*

Institute of Nanoscience and Nanotechnology, Central China Normal University, Wuhan 430079, China

Manganese dioxide (MnO_2) films with different nanostructures were deposited on indium tin oxide (ITO) glasses by using chemical bath deposition (CBD). Deposition temperature and time were varied from 60 °C to 90 °C and from 2 h to 72 h, respectively. The samples have been characterized using an X-ray diffraction (XRD), field emission scanning electron microscope (SEM) and an electrochemical workstation. The films deposited at 60 °C for 8 h showed that obtained nanoflowers had an amorphous nature, while those deposited at higher temperatures of 70, 80 and 90 °C showed a well-developed nanowire and nanorod morphology. However, those which were deposited at 60 °C, showed the best electrochemical properties, including a higher specific capacitance, good rate of performance and a cycling stability (93 % loss of the initial value after 10,000 cycles).

Keywords: *thin film; energy storage; chemical bath deposition; bath temperature; electrochemical properties*

1. Introduction

Manganese dioxide (MnO_2) is one of the most attractive transition metal oxides that have been employed as redox catalysts and especially as electroactive material in electrochemical capacitors and batteries. This is due to its great abundance, low cost, favorable charge density, high electrochemical and chemical stability as well as low toxicity. It is well known that the particle size and surface morphology of MnO_2 can influence its electrochemical performance. MnO_2 has attracted much attention because of its particular physical and chemical properties. In addition, it possesses great potentials in such applications as selective heterogeneous catalysts, adsorbents, and battery materials [1]. Various forms of MnO_2, including one-dimensional (nanorods, nanowires, nanotubes) [2, 3], two-dimensional (2-D) (nanosheets, nanoflakes) [4, 5], and three-dimensional (3-D) (nanospheres, nanoflowers) [6] nanostructures have been synthesized. By contrast, 3-D hierarchical MnO_2 structures are more preferable for various applications due to their production of more reaction-active sites than in 1-D and 2-D structured materials. In addition, they exhibit more favorable electrochemical properties [7]. Moreover, 3-D electrode materials facilitate the penetration of both electrolytes and reactants into the whole oxide matrix in order to maintain very smooth electron pathways in rapid charge-discharge reactions [8]. Preparation conditions for MnO_2 materials have a great influence on their physico-chemical properties, including nanostructures, morphology as well as chemical composition and porosity, which have an impact on important electrochemical activities [9–13]. The nature of the reactants, pH of the reaction medium, heating temperature and heating duration have all dramatic effects on the crystal structures of the phases formed [14].

Thin films prepared by chemical methods are generally less expensive than those prepared by physical, capital-intensive techniques. We selected a chemical bath deposition method due to its numerous advantages, such as low cost, large area production and simplicity in instrumental operation. The chemical bath deposition facilitates the

*E-mail: ywtang@phy.ccnu.edu.cn

control of growth factors, like film thickness, deposition rate and quality of crystallites by varying such parameters as pH of solution, temperature, and bath concentration [15]. In the experiments carried out, MnO_2 nanoflowers, nanowires and nanorods were all grown on an indium tin oxide (ITO) substrate by a CBD method. The influence of the reaction bath time and bath temperature on the growth process and capacitive behaviors of the MnO_2 thin films was investigated.

2. Experimental

MnO_2 thin films were deposited on ITO glass substrates at different deposition bath temperatures (60, 70, 80 and 90 °C). The substrates of ITO glass were ultrasonically cleaned in distilled water, acetone and absolute ethanol, for 10 minutes in each solvent, and then dried at a room temperature. For the deposition of MnO_2 thin films, 30 mL of 1 M manganese sulfate ($MnSO_4{\cdot}H_2O$), 30 mL of 1 M potassium persulfate ($K_2S_2O_8$) and 30 mL of 1 M sodium sulfate (Na_2SO_4) were used. The bath temperature was fixed at an appropriate temperature, then the pre-cleaned substrates were submerged into the solution, while this latter was magnetically stirred in a beaker for 8 h. After completion of the film deposition, the samples were taken out, immediately rinsed with deionized water to remove soluble impurities and then dried in a vacuum at 60 °C overnight. To investigate the influence of deposition time, the above steps were repeated at different reaction bath times (2, 4, 6, 8, 12, 24, 48 and 72 h) at 60 °C.

The phase purity of the samples was characterized by X-ray powder diffraction (XRD) using an X-ray diffractometer (Y-2000) with Cu Kα radiation (λ = 1.5418 Å). Scanning electron microscopy (SEM) images were obtained on a JEOL JSM-6700F microscope operated at 5 kV. Electrochemical measurements were carried out in an electrochemical workstation (CHI440A Instruments, Chenhua Co., Shanghai) using a conventional three-electrode electrochemical cell with a 0.5 M of Na_2SO_4 aqueous solution as the electrolyte. The MnO_2 film was used as the working electrode, whereas a platinum foil and saturated calomel electrode (SCE) were used as counter and reference electrodes, respectively.

3. Results and discussion

3.1. XRD

The XRD patterns of the MnO_2 samples, prepared at different reaction times (2, 4, 6, 8, 12 and 24 h), are shown in Fig. 1a. The diffraction peaks of the as prepared MnO_2 samples at 2θ = 27.53, 36.83, 41.23, 50.68, and 53.30° correspond to the Miller indices or lattice planes of (1 2 0), (0 2 1), (2 1 0), (0 4 1), and (1 5 0), respectively. Therefore, they can be indexed to the tetragonal ramsdellite (JCPDS card No. 7-222), whereas the peaks at 2θ = 32.96, 60.66 and 64.08° are indexed to Mn_2O_3 (JCPDS card No. 124-508). The peaks marked with "*" can be attributed to the substrate. The less intensity of the diffracted peaks reveales the low crystallinity of the as prepared samples. The calculated average crystallite sizes of the MnO_2 prepared at 70 °C are 30, 32, 25, 27, 28 and 22 nm for the samples prepared for 2, 4, 6, 8, 12 and 24 h, respectively. It is clear that the intensity of the diffraction peaks decreased, and the full width of the half maximum (FWHM) intensity increased with prolonging the bathing time, which indicates that the crystallinity of the films decreased gradually.

Fig. 1b shows the XRD patterns of the MnO_2 films deposited on ITO glass substrates at different bath temperatures of 60, 70, 80 and 90 °C for 8 h. Except for the peaks marked with "*", which can be attributed to the ITO glass substrate, the all observed diffraction peaks at 27.4°, 38.6° and 55.3° correspond to the planes of (1 2 0), (0 4 0), and (2 2 1) of manganese dioxide. They have been readily indexed to the tetragonal ramsdellite MnO_2 (JCPDS card No. 5-600). The intensity of the diffraction peaks decreased with the increase of the bath temperature, indicating that the crystallinity degree depends on the temperature. The MnO_2 films deposited at 80 and 90 °C were well crystallized, while those that were deposited at 60 and 70 °C were poor crystalline, as it is indicated by the larger, broader peak from 20 to 35° in the

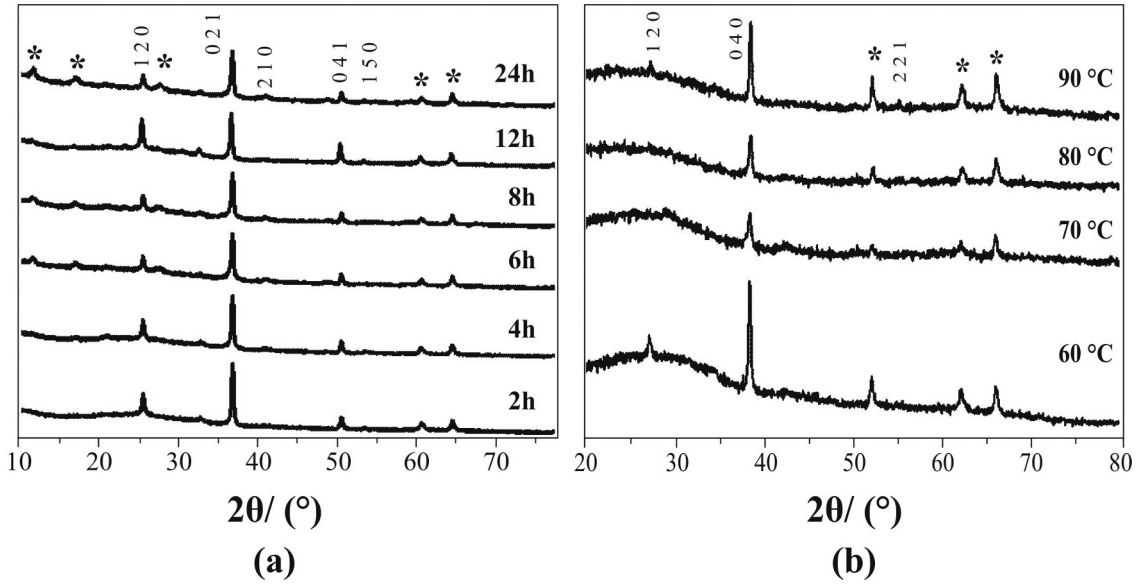

Fig. 1. XRD patterns of MnO_2 films deposited on ITO glass (a) at different times: 2, 4, 6, 8, 12, 24 and 48 h, at 60 °C, (b) at various bath temperatures: 60, 70, 80 and 90 °C for 8 h.

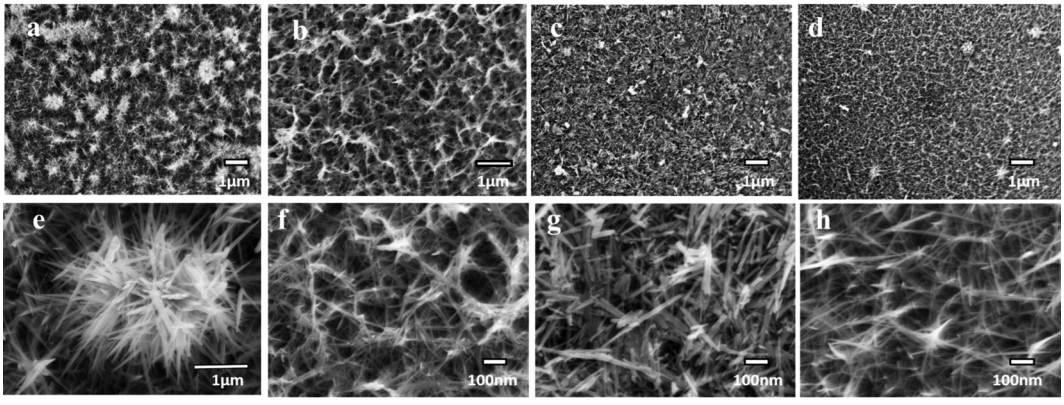

Fig. 2. SEM images of MnO_2 deposited on ITO glass at different bath temperatures: (a) 60 °C, (b) 70 °C, (c) 80 °C and (d) 90 °C; (e), (f), (g) and (h) are the enlarged images of (a), (b), (c) and (d), respectively.

XRD patterns of these samples. It is worth mentioning that the amorphous phase of the oxide material is generally necessary to have an electrode with large surface area for supercapacitor applications [16]. Meanwhile, the XRD results revealed that bath temperatures had a significant effect on the recorded XRD patterns of the deposited films.

3.2. SEM

The surface morphologies of MnO_2 deposited at various bath temperatures 60, 70, 80 and 90 °C, resemble nanoflowers (Fig. 2a), nanowires (Fig. 2b) nanorods (Fig. 2c) and nanowires (Fig. 2d), respectively. The magnified FESEM image (Fig. 2e) shows that the nanoflowers consist of nanowhiskers radiating from the center. Fig. 2f shows that the nanowires have a length of 1 μm and a diameter of 70 nm, and Fig. 2h shows that the nanowires have a length of 2 μm and a diameter of 100 nm. The diversity of MnO_2 structures formed at various bath temperatures can be explained by reaction kinetics. The kinetics manipulation is a versatile approach to control the morphology and

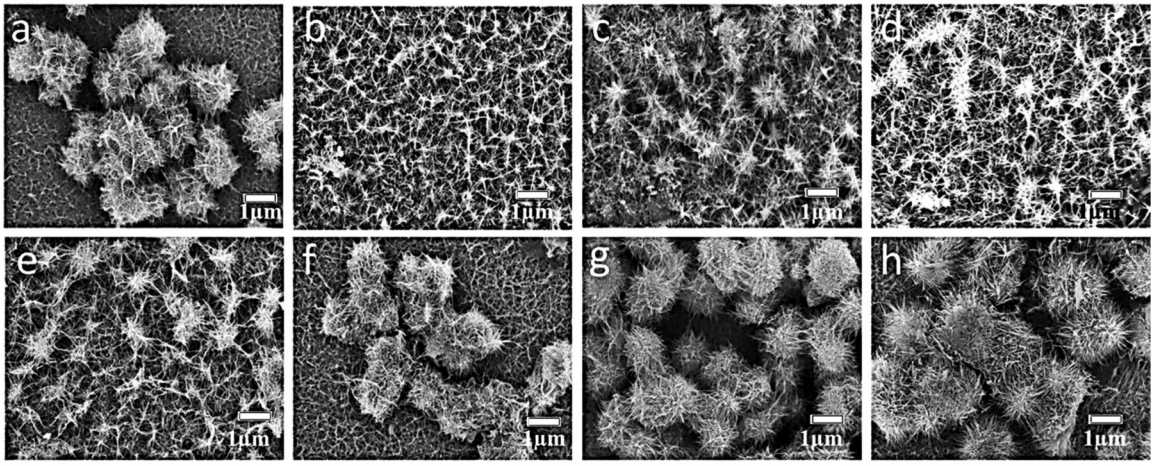

Fig. 3. SEM images of MnO_2 nanofollowers grown on ITO glass at 60 °C. at different times: (a) 2, (b) 4, (c) 6, (d) 8, (e) 12, (f) 24, (g) 48, and (h) 72 h.

shape of nanostructures. The increase of temperature had a strong impact on the diameter, length and pore size of the nanowires. The average diameter and length increased dramatically with the increase in temperature.

The surface morphology of MnO_2 films deposited on ITO glass substrates at 60 °C after different bath times is shown in (Fig. 3). Several obvious evolution stages could be clearly observed. In the initial stage, Fig. 3a (the shortest reaction time, 2 h), only a close-grained spheres are observed; after a bath reaction for 6 h, as shown in Fig. 3c, the MnO_2 spheres have changed to a flower-like nanostructures, which consist of nanowhiskers and nanowires. When the reaction time was prolonged to 24 h (Fig. 3f), the morphology returned back to the close-grained spheres and with a further prolonging reaction time of 48 h and 72 h, the surface of the MnO_2 spheres has changed into a sea-urchin like (Fig. 3g and 3h).

In order to explore other parameters that might have different impacts on the morphology of the products, we chose a sample synthsized at 70 °C for 2 h, and elongated the reaction time to 24 h. As it is revealed in Fig. 4, the length of time has not led to a big variation in the morphology of the MnO_2, but the dispersity and uniformity became better with the increase of the reaction time. Further, the surface of the MnO_2 nanorod seems to be more uniform and smoother, and no other impurities on the surface are observed.

3.3. Electrochemical performance

Both the C-V and EIS (Electrochemical Impedance Spectroscopy) measurements were applied to evaluate the electrochemical properties of the as-prepared electrode samples. Fig. 5a shows the C-V curves of the MnO_2 films deposited at different bath temperatures of 60, 70, 80 and 90 °C for 8 h, measured in a 0.5 M of Na_2SO_4 electrolyte at a scan rate of 50 $mV{\cdot}s^{-1}$. It is clear that all of the C-V curves for the MnO_2 electrode are almost ideally rectangular, exhibiting the typical electrochemical capacitive behavior with a very rapid current response to voltage reversal at each end potential, and high reversibility [17, 18]. Evidently, the MnO_2 nanoflower film electrodes, deposited at 60 °C, show a higher integrated area than the MnO_2 nanorod films and MnO_2 nanowires electrodes deposited at 70, 80 and 90 °C. This indicates their excellent electrochemical performance. The specific capacitances were calculated from the C-V curves according to the following equation:

$$C_S = \frac{\int IdV}{2\nu\Delta Vm} \tag{1}$$

where I (A) stands for the response current, ν ($V{\cdot}s^{-1}$) is the potential scan rate, ΔV (V) is the potential window, and m (g) is the mass of

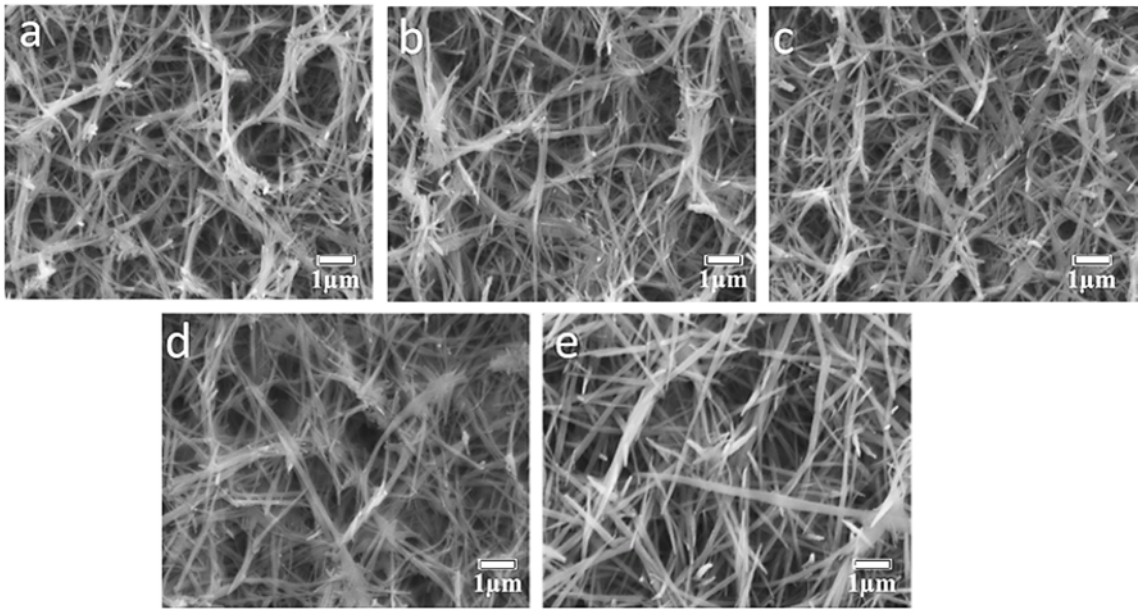

Fig. 4. SEM images of MnO_2 nanorods grown on ITO glass at 70 °C at different times: (a) 2, (b) 4, (c) 8, (d) 12 and (e) 24 h.

active electrode material. The calculated specific capacitances of the MnO_2 nanoflower film electrode, MnO_2 nanorod electrode and MnO_2 nanowires, measured at 40 $mV \cdot s^{-1}$, are 423, 301, 292 and 260 Fg^{-1}. EIS measurements were performed in order to further evaluate the electrochemical properties of the MnO_2 nanoflower, MnO_2 nanorod and MnO_2 nanowire electrodes. Typical Nyquist plots of EIS for these electrodes are presented in Fig. 5b. There are straight lines in the low-frequency region, and semicircles in the high frequency one. At a low frequency, the imaginary part sharply increases, and a vertical line can be observed, indicating a pure capacitive behavior [19]. The intersection of the semicircle on the real axis at a high frequency represents the equivalent series resistance (R_s) of the electrode, while the diameter of the semicircle corresponds to the charge-transfer resistance (R_{ct}) at the electrode and electrolyte interface [20]. Comparing the impedance plots of these electrodes, it is apparent that the values of R_{ct} and R_s gradually increase, while the bath temperature increases. The charge-transfer resistance (R_{ct}) and the equivalent series resistance (R_s) of the MnO_2 nanoflower are smaller than that of the MnO_2 nanorods and MnO_2 nanowires, which suggests that the MnO_2 nanoflower has better conductive properties and, therefore, a better electrochemical behavior. It can be seen that the straight line of the MnO_2 nanoflower in a low frequency range, nearly vertical to the real impedance axis (Z') is observed as a characteristics of the excellent capacitive behavior. Deviation from the vertical line could be ascribed to the inner-mesoporous diffusion resistance of electrolyte ions, which is strongly dependent on a particular mesoporous structure [21]. It is speculated that the low resistance of the MnO_2 nanoflower electrode is due to its high specific surface area, which facilitates a faster cation insertion and extraction during the charge-discharge process [22]. To get more information on the capacitive performance of the as-prepared samples, a MnO_2 nanoflower electrode was selected for detailed measurements. Fig. 5c illustrates the C-V curves of this electrode measured at different scan rates of 3, 5, 10, 20, 40, 50 and 60 $mV \cdot s^{-1}$ in 0.5 M of Na_2SO_4 electrolyte. All the C-V curves are close to a rectangular shape with high symmetry features, indicating ideal capacitive properties and

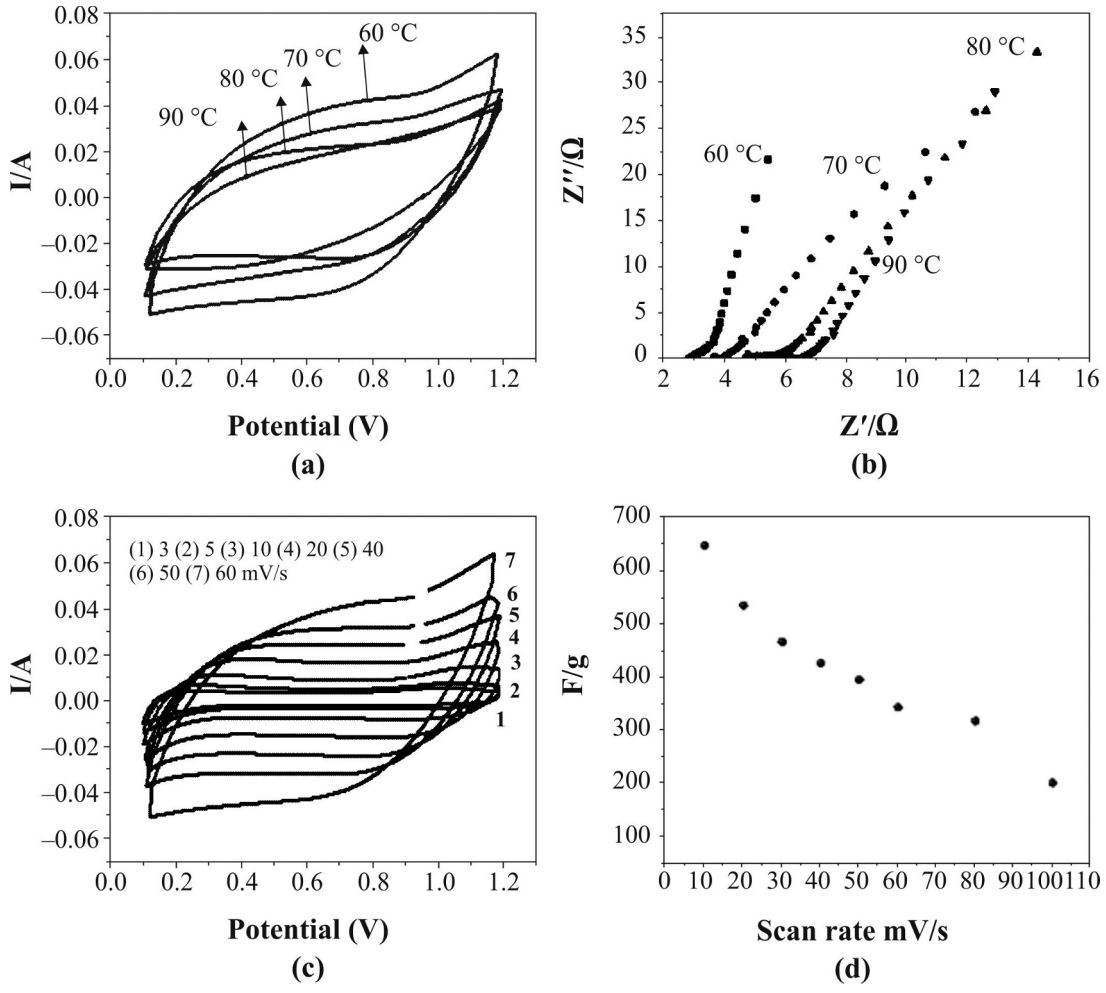

Fig. 5. (a) C-V curves of MnO_2 thin films deposited at 60, 70, 80 and 90 °C for 8 h, measured at a scan rate of 40 $mV \cdot s^{-1}$ in 0.5 M Na_2SO_4 electrolyte; (b) Nyquist plots of MnO_2 thin films deposited at 60, 70, 80 and 90 °C for 8 h; (c) C-V curves of the electrode from MnO_2 thin films deposited at 60 °C, measured at different scan rates in 0.5 M of Na_2SO_4 electrolyte; (d) the specific capacitance as a function of potential scan rate.

an excellent reversibility of this electrode. The specific capacitance values as a function of potential scan rate are presented in Fig. 5d. The specific capacitance values calculated from different scan rates are 651, 538, 469, 429, 398, 346, 320 and 203 $F \cdot g^{-1}$ at 10, 20, 30, 40, 50, 60, 80 and 100 $mV \cdot s^{-1}$, respectively, exhibiting the large specific capacitances and a good power capability of the electrode. In addition, it can be observed that the specific capacitance of the MnO_2 nanoflower electrode decreased with the increase of a scan rate ranging from 10 $mV \cdot s^{-1}$ to 100 $mV \cdot s^{-1}$. The reason is that at high scan rates the concentration of ions on the solid-liquid interface increases rapidly and the diffusion rate of electrolyte from the solid-liquid interface to the electrode material is not fast enough to satisfy the electrochemical reactions of the electrode material [23]. Therefore, this results in the enrichment of the electrolyte near the solid-liquid interface and the polarization of the electrode, which then leads to a drop in the specific capacitance of the supercapacitor [24]. Meanwhile, the decreasing trend of the specific capacitance indicates that parts of the surface of the electrode are inaccessible at high charge-discharge rates by the electrolyte [25]. The C-V curves at different

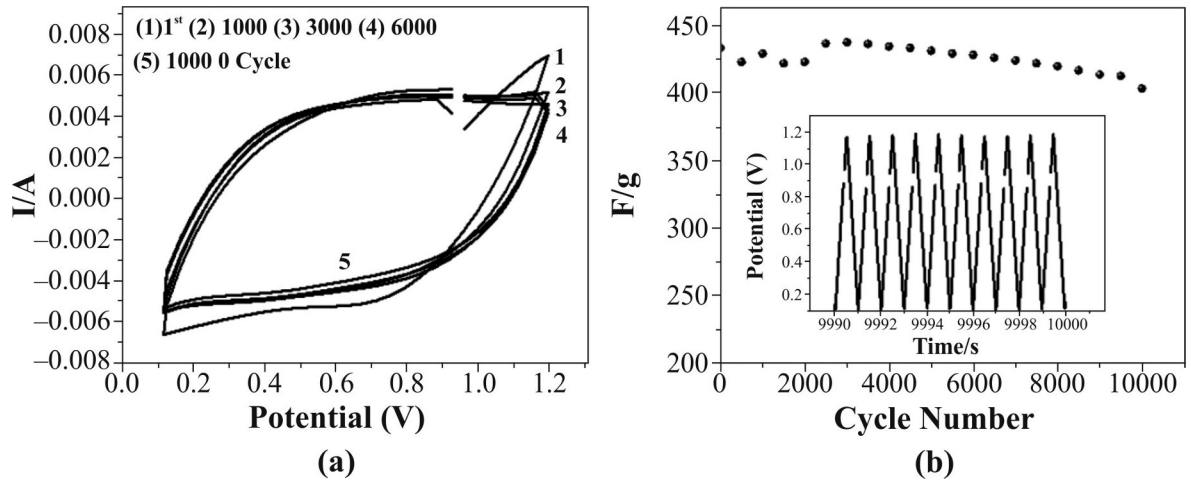

Fig. 6. Measurement results for MnO_2 nanoflower thin film synthesized at 60 °C (a) C-V curves for the 1st, 1000th, 3,000th, 6,000th and 10,000th cycles measured at a scan rate of 40 $mV \cdot s^{-1}$, (b) variation of specific capacitance with respect to cycle number. The inset shows the galvanostatic charge-discharge curve.

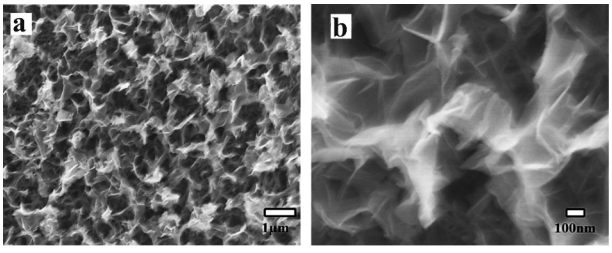

Fig. 7. (a) SEM images of MnO_2 thin film synthesized at 60 °C after the 10,000th cycles; (b) enlarged images of (a).

cycling stages and a variation of specific capacitance over 10,000 cycles are shown in Fig. 6. As shown in Fig. 6a, the C-V curves for the 1st, 1000th, 3,000th, 6,000th and 10,000th cycles almost overlap each other, indicating an excellent cycling stability. The C-V curve after 1,000 cycles is noted to become more symmetrical with even more rectangular shape compared with the first cycle indicating an improved capacitive behavior after a long-term cycling. After 2,000 cycles there is no degradation of the capacitive behavior indicating no significant structural or microstructural changes in the MnO_2 thin film electrodes. The electrochemical stability is important for supercapacitors [26, 27]. Fig. 6b illustrates the capacitance performances of the MnO_2 nanoflower thin film electrode as a function of cycle numbers at a scan rate of 40 $mV \cdot s^{-1}$. The specific capacitance of the MnO_2 nanoflower electrode slightly increased and then stabilized at around the 1,500th cycle and still remained at 93 % of the initial capacitance after 10,000 charge-discharge cycles, demonstrating an excellent long-term cycling stability. This is attributed to more accessible porous surfaces to electrolyte ions after a number of cycles. Thus, the effective surface area increased and the capacitance improved. The inset has not revealed any significant electrochemical change during the long-term charging and discharging processes after 10,000 times cycling. The morphology was studied by SEM after 10,000 potential cycles, (Fig. 7). The MnO_2 nanoflower electrode was converted into porous snowflake morphology. Electroactive material of higher porosity lead to an enhanced utilization by facilitating faradaic reactions through the intercalation of protons/electrolyte cations into the bulk phase of the MnO_2 electrode [28]. The penetration depth of electrolyte cations depends greatly on the porosity of the electrode matrix [29]. Besides, such surface morphological transformation could lead to improved capacitive behaviors of the MnO_2 electrode due to a reduction in the interparticle contact resistance and hence, a higher electrical conductivity. Therefore, the improvement of SC should be ascribed to the morphological changes.

Fig. 8 shows the cyclic voltammograms of the MnO_2 films of nanoflower, nanorod and nanowires

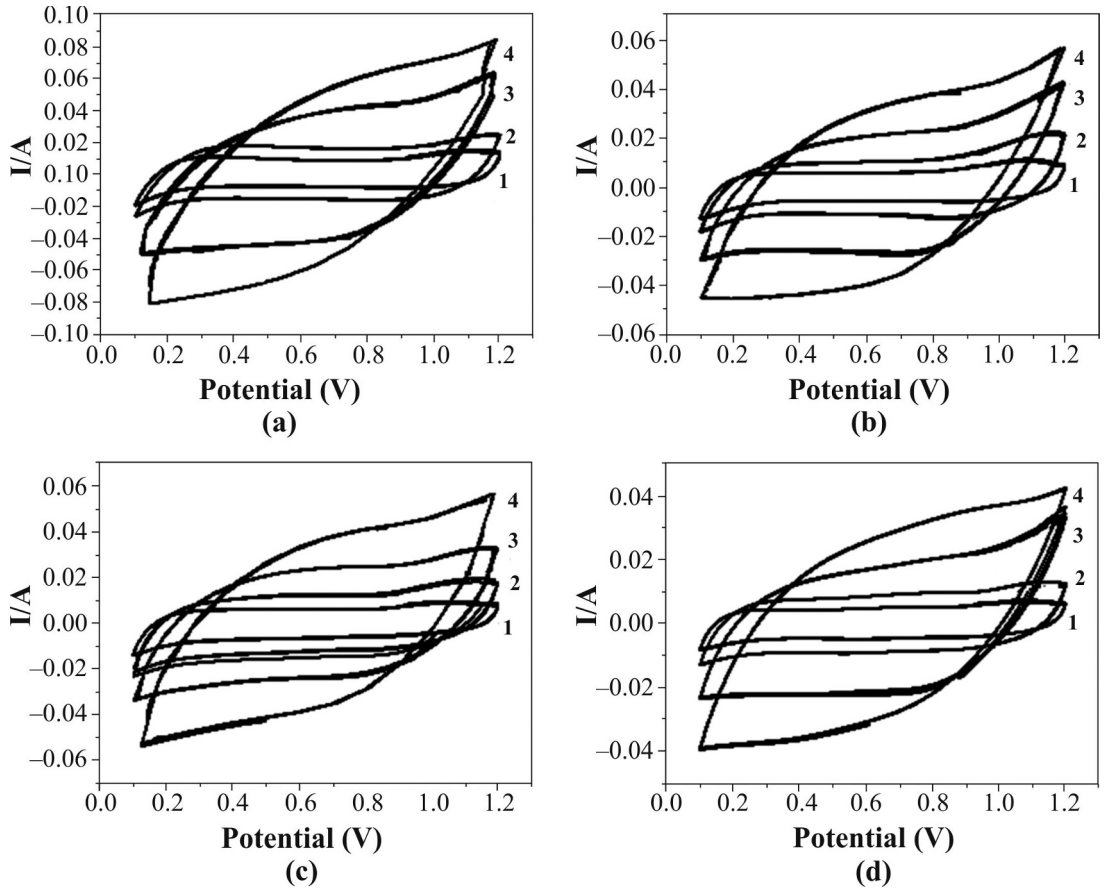

Fig. 8. Cyclic voltammograms of the MnO_2 films (a) with nanoflower structure, deposited at 60 °C, (b) nanowires deposited at 70 °C, (c) nanorods deposited at 80 °C, and nanowires deposited at 90 °C, and (d) in the scan rates of (1) 10 $mV \cdot s^{-1}$, (2) 20 $mV \cdot s^{-1}$, (3) 50 $mV \cdot s^{-1}$ and (4) 100 $mV \cdot s^{-1}$.

deposited at 60, 70, 80 and 90 °C at different scan rates (10 $mV \cdot s^{-1}$, 20 $mV \cdot s^{-1}$, 50 $mV \cdot s^{-1}$ and 100 $mV \cdot s^{-1}$). Fig. 8 shows that the nanoflower and nanowire films have higher capacitances than the nanorod films at a cyclic rate of 40 $mV \cdot s^{-1}$ due to the fact that both nanoflower and nanowires films have higher surface areas than that of nanorod ones. The nanoflower films have the largest area of cyclic voltammograms at the highest scan rate of 100 $mV \cdot s^{-1}$, showing that higher surface ratio can provide the higher capacitance. Moreover, the nanoflower films have the best cyclic voltammograms in the whole range of scan rates, indicating that the nanoflower films have the best charge and discharge efficiencies [30].

The MnO_2 prepared by CBD at 60, 70, 80, and 90 °C for 8 h were subjected to an extended charge-discharge cycling at 1 Ag^{-1} in the 0.5 M of Na_2SO_4 electrolyte and the result is depicted in Fig. 9. The SC could be calculated from:

$$C = \frac{I \times \Delta t}{\Delta V \times m} \tag{2}$$

where C, I, Δt, ΔV and m stand for the specific capacitance, galvanostatic current, charge/discharge time, potential cut-off window and mass of the electro-active material. The specific capacitance of the MnO_2 prepared at 60 °C was found to be 229 $F \cdot g^{-1}$ after 1000 cycles, which indicates that the capacitance value of this film is higher than the one of the films prepared at 70 °C, 80 °C and 90 °C, (213 $F \cdot g^{-1}$, 205 $F \cdot g^{-1}$, 180 $F \cdot g^{-1}$, respectively). This can be attributed to the MnO_2 nanoflowers uniformly dispersed over the surface of ITO, which provided a reasonable rate capability during

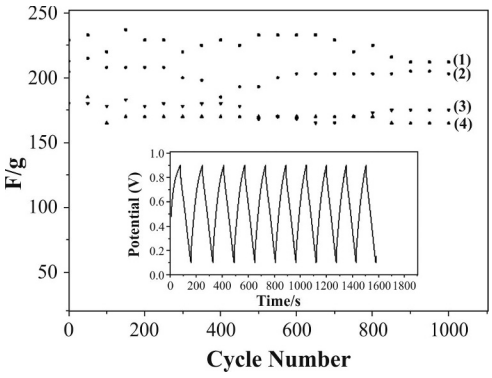

Fig. 9. Cycle performance of MnO_2 electrod temperatures (1) 60 °C, (2) 70 °C, (3) 80 °C, and (4) 90 °C. The inset shows the last 10 cycles of galvanostatic charge-discharge.

the reversible conversion reaction. The nearly symmetric charge and discharge curves of the last 10 cycles (inset in Fig. 9) confirm the high activity and reversibility of MnO_2 nanoflowers prepared at 60 °C.

4. Conclusion

To sum up, CBD has been proved to be a practical method for the deposition of oxide thin films at low temperatures, and it may be extended to fabricate other oxide thin films. MnO_2 thin films were deposited on ITO glass substrates by CBD method directly from an aqueous solution in a temperature range of 60 to 90 °C. It was found that the floating substrate is beneficial for high-quality thin films during the CBD procedure. The reaction temperature was an important mean to control the morphology and shape of the nanostructures. The MnO_2 films deposited at 80 and 90 °C were well crystalline, while those deposited at 60 and 70 °C were poor crystalline. At the reaction temperature of 60 °C and reaction time of 8 h, a film of 3-D MnO_2 nanoflowers was formed. However, the increase of the reaction temperature has not resulted in improving the formation of 3-D MnO_2 nanoflowers, but it led to the formation of 1-D nanowires and nanorods. The film composed of 3-D MnO_2 nanoflowers exhibited a higher specific capacitance and better rate capability than that, which was composed of 1-D porous nanowires and nanorods. This was probably due to the high surface area and amorphous phase. To study the effect of time, we chose the sample synthsized at 60 °C for 2 h and elongated the reaction time to 48 h. As it was revealed, lengthening the time did not lead to a big variation in the morphology of MnO_2, but dispersity and uniformity became better with the increase of the reaction time. The surface of the MnO_2 nanfllowers was also more uniform and smoother, and hence, no other impurities on the surface were observed.

Acknowledgements

This work was financially supported by the Key Project of Natural Science Foundation of Hubei Province (No. 2012EFA080) and the National Ministry of Science and Technology under Grant No. 2011YQ160002.

References

[1] Ai Z., Zhang L., Kong F., Liu H., Xing W., Qiu J., *Mater. Chem. Phys.*, 111 (2008), 162.
[2] Liu Y., Zhang M., Zhang J., Qian Y., *J. Solid State Chem.*, 179 (2006), 1757.
[3] Xiao W., Xia H., Fuh J.Y.H., Lu L., *J. Power Sources*, 193 (2009), 935.
[4] Wei L., Li C., Chu H., Li Y., *Dalton T.*, 40 (2011), 2332.
[5] Li J., Wang N., Zhao Y., Ding Y., Guan L., *Electrochem. Commun.*, 13 (2011), 698.
[6] Hou Y., Cheng Y., Hobson T., Liu J., *Nano Lett.*, 10 (2010), 2727.
[7] Si P., Chen P., Kim D.H., *J. Mater. Chem. B*, 1 (2013), 2696.
[8] Yang G., Wang B., Guo W., Bu Z., Miao C., Xue T., Li H., *Mater. Res. Bull*, 47 (2012), 3120.
[9] Ding K.Q., *Int. J. Electrochem. Sc.*, 5 (2010), 72.
[10] Kim S.H., Kim Y.I., Park J.H., Ko J.M., *Int. J. Electrochem. Sc.*, 4 (2009), 1489.
[11] Jayalakshmi M., Balasubramanian K., *Int. J. Electrochem. Sc.*, 3 (2008), 1196.
[12] Adelkhani H., Ghaemi M., Jafari S.M., *J. Power Sources*, 163 (2007), 1091.
[13] Adelkhani H., *J. Electrochem. Soc.*, 156 (2009), 791.
[14] Ghaemi M., Biglari Z., Binder L., *J. Power Sources*, 102 (2001), 29.
[15] Kathalingam A., Ambika N., Kim M.R., Elanchezhiyan J., Chae Y.S., Rhee J.K., *Mater. Sci.-Poland*, 28 (2010), 513.
[16] Dubal D.P., Dhawale D.S., Gujar T.P., Lokhande C.D., *Appl. Surf. Sci.*, 257 (2011), 3378.
[17] Prasad K.R., Miura N., *Electrochem. Commun.*, 6 (2004), 1004.

[18] WU M., SNOOK G.A., CHEN G.Z., FRAY D.J., *Electrochem.Commun.*, 6 (2004), 499.
[19] BISWAS S., DRZAL L.T., *Chem. Mater.*, 22 (2010), 5667.
[20] XIONG W., LIU M.X., GAN L.H., LV Y.K., LI Y., YANG L., *J. Power Sources.*, 196 (2011), 10461.
[21] WANG D.W., LI F., CHENG H.M., *J. Phys. Chem. B*, 110 (2006), 8570.
[22] ZHANG K., ZHANG L.L., ZHAO X.S., WU J., *Chem. Mater.*, 22 (2010), 1392.
[23] XU C.H., SUN J., GAO L., *J. Mater. Chem.*, 21 (2011), 11253.
[24] DUBAL D.P., KIM W.B., LOKHANDE C.D., *J. Phys. Chem. Solids*, 73 (2012), 18.
[25] GUJAR T.P., SHINDE V.R., LOKHANDE C.D., HAN S.H., *J. Power Sources*, 161 (2006), 1479.
[26] BI R.R., WU X.L., CAO F.F., JIANG L.Y., GUO Y.G., WAN L.J., *J. Phys. Chem.*, 114 (2010), 2448.
[27] LI J., LIU E.H., LI W., MENG X.Y., TAN S.T., *J. Alloy. Compd.*, 478 (2009), 371.
[28] SIMON P., GOGOTSI Y., *Nat. Mater.*, 7 (2008), 845.
[29] QU D.Y., *J. Power Sources*, 102 (2001), 270.
[30] WU M.S., LEE J.T., WANG Y.Y., WAN C.C., *J. Phys. Chem.*, 108 (2004), 16331.

Received 2014-04-01
Accepted 2014-07-02